AD

TECHNICAL REPORT ARCCB-TR-93022

MEASUREMENT AND THEORY OF THE DEPENDENCE OF HARDNESS ON RESIDUAL STRESS

A. ABBATE
J. FRANKEL
W. SCHOLZ

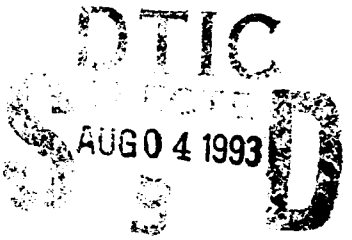

MAY 1993

US ARMY ARMAMENT RESEARCH,
DEVELOPMENT AND ENGINEERING CENTER
CLOSE COMBAT ARMAMENTS CENTER
BENÉT LABORATORIES
WATERVLIET, N.Y. 12189-4050

APPROVED FOR PUBLIC RELEASE; DISTRIBUTION UNLIMITED

DISCLAIMER

The findings in this report are not to be construed as an official Department of the Army position unless so designated by other authorized documents.

The use of trade name(s) and/or manufacturer(s) does not constitute an official indorsement or approval.

DESTRUCTION NOTICE

For classified documents, follow the procedures in DoD 5200.22-M, Industrial Security Manual, Section II-19 or DoD 5200.1-R, Information Security Program Regulation, Chapter IX.

For unclassified, limited documents, destroy by any method that will prevent disclosure of contents or reconstruction of the document.

For unclassified, unlimited documents, destroy when the report is no longer needed. Do not return it to the originator.

REPORT DOCUMENTATION PAGE

Form Approved
OMB No. 0704-0188

1. AGENCY USE ONLY (Leave blank)	2. REPORT DATE	3. REPORT TYPE AND DATES COVERED
	May 1993	Final

4. TITLE AND SUBTITLE
MEASUREMENT AND THEORY OF THE DEPENDENCE OF HARDNESS ON RESIDUAL STRESS

5. FUNDING NUMBERS
AMCMS: 612624H180.0
PRON: 479TE102471A

6. AUTHOR(S)
A. Abbate, J. Frankel, and W. Scholz (Benet and State University of New York at Albany)

7. PERFORMING ORGANIZATION NAME(S) AND ADDRESS(ES)
U.S. Army ARDEC
Benet Laboratories, SMCAR-CCB-TL
Watervliet, NY 12189-4050

8. PERFORMING ORGANIZATION REPORT NUMBER
ARCCB-TR-93022

9. SPONSORING / MONITORING AGENCY NAME(S) AND ADDRESS(ES)
U.S. Army ARDEC
Close Combat Armaments Center
Picatinny Arsenal, NJ 07806-5000

10. SPONSORING / MONITORING AGENCY REPORT NUMBER

11. SUPPLEMENTARY NOTES

12a. DISTRIBUTION / AVAILABILITY STATEMENT
Approved for public release; distribution unlimited.

12b. DISTRIBUTION CODE

13. ABSTRACT *(Maximum 200 words)*
The Rockwell C hardness (R_C) was measured as a function of position on the three steel rings cut from tubes with different amounts of autofrettage. These rings had different residual stress profiles through the wall that were measured using an ultrasonic technique. An experimental correlation between residual stress and R_C was obtained. In order to model the effects of residual stress on the measured hardness, the Tresca (linear) and the von Mises-Hencky (power) yield criteria were utilized within a model given by Shaw, Hoshi, and Henry that depicts the stress state within a spherical indenter. The von Mises-Hencky method was more successful in matching the data.

14. SUBJECT TERMS	15. NUMBER OF PAGES
Hardness, Residual Stress, Yielding Criteria, Autofrettage, Ultrasonics	27
	16. PRICE CODE

17. SECURITY CLASSIFICATION OF REPORT	18. SECURITY CLASSIFICATION OF THIS PAGE	19. SECURITY CLASSIFICATION OF ABSTRACT	20. LIMITATION OF ABSTRACT
UNCLASSIFIED	UNCLASSIFIED	UNCLASSIFIED	UL

TABLE OF CONTENTS

Tables

List of Illustrations

ACKNOWLEDGEMENTS

It is a pleasure to thank W. Korman for his ubiquitous help, B. Brown for helpful conversations and specimens, and J. Underwood for sharing his experience in the field.

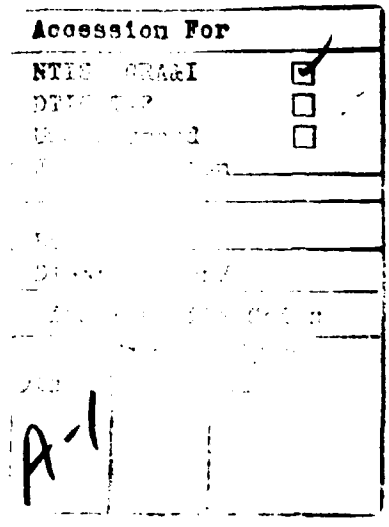

INTRODUCTION

Hardness tests are useful and easy to perform, but they are difficult to understand. By modelling the effect of residual stresses on the measured hardness, we hope to sharpen our fundamental understanding of the effect of various material parameters on hardness, or conversely, our ability to extricate material parameters from hardness tests. In addition, the authors, along with previous investigators (refs 1-4), project the future use of hardness tests to measure or correct for surface residual stresses in materials. We present a model to evaluate the effect of residual stress on the measured hardness. This model is subsequently used to fit our experimental data, and a final relationship is obtained. In particular, our model found the Rockwell C (R_C) hardness as a function of the radial (σ_R) and hoop (σ_H) residual stresses and the yield strength (Y). A fitting parameter (α) was introduced to scale the effect of the direction of the pressure between the ball and the specimen (p) with respect to the residual stress.

We obtained the experimental data from steel specimens that contained a large range of well-characterized residual stresses: over 50 percent of yield strength in compression and more than 30 percent of yield strength in tension.

EXPERIMENTAL DETAILS

Right circular cylinders (Figure 1) were measured. These cylinders were hollow and symmetrical, and they were cut out of steel tubes that were previously autofrettaged. This process provides a residual stress that is compressive at the inside diameter (ID) and tensile at the outside diameter (OD). The flat cylinder faces were ground smooth and parallel for ultrasonic measurements, which were performed first. Three samples with different amounts of autofrettage were measured:

1. Sample G - the autofrettage process was extended up to 80 percent of its thickness.

2. Sample FC6355 - the autofrettage process was extended up to 40 percent of its thickness.

3. Sample 100 - the autofrettage process was extended up to 100 percent of its thickness.

The last two samples came from the same material and underwent the same heat treatment but were subjected to different amounts of autofrettage (ref 5).

Shear ultrasonic waves with the polarization in the hoop direction and propagation in the axial direction were used to obtain the residual stresses (refs 6,7). X-ray residual stress data had also been taken on specimen G, which provided good agreement with the ultrasonic results.

The measured hoop residual stresses versus position for the three tubes are given in Figures 2, 3, and 4. These figures also contain the analytically obtained radial stresses for these tubes (ref 8) comparable to the autofrettage measured ultrasonically as described above. The corresponding R_C readings are found in Figures 5, 6, and 7. In each case, these readings were taken in four lines one-eighth inch apart parallel to the radial direction in the tube and averaged for each radial position. Successive points in each line were also at least one-eighth inch apart. The average value of hardness for each position was used in our successive calculations.

THEORY AND BACKGROUND

In order to obtain the relationship between the measured hardness and the residual stress, Figure 8a depicts how the residual stress in our specimen affects the stress directly below a spherical indenter (point A in Figure 8b). In this case, p is the normal stress (assuming zero friction) applied by the spherical indenter to the specimen, and σ_H and σ_R are as defined previously. This depiction without residual stresses is given by Shaw, Hoshi, and Henry (ref 9), and it is related to the situation in which the load W is still applied, but the deformation has stopped. We use the stresses depicted in Figure 8a in the von Mises-Hencky and the Tresca criteria for yielding to calculate the pressure p, which would cause yielding. The Meyer hardness is a measurement of this pressure, which we then convert to R_C to compare with our experimental data. We found, however, that the simplifying assumption in which the pressure p and the residual stresses σ_H and σ_R add up, as depicted in Figure 8b for the whole surface of the ball indenter, overestimated the effect of the residual stress on our calculated hardness. Therefore, we incorporated a fitting parameter α into our equations as the coefficient of the residual stress.

Hardness Concepts and Conversions

Conversions between various hardness numbers have to be used carefully. We used conversions between three hardness numbers applicable for steels in our hardness range. These are discussed briefly below:

1. The Rockwell C hardness, R_C, is determined as a diamond indenter in the shape of a right circular cone with a 120-degree tip angle, and a 0.2-mm tip radius is pushed at right angles into a smooth steel surface. Initially, a 10-Kg weight and subsequently, a 140-Kg weight are added and then removed. The depth of indentation h (mm) after the release of the 140-Kg weight is measured, and R_C is obtained as follows:

$$R_C = 100 - \frac{h}{0.002} \tag{1}$$

2. The Brinell test is conducted by loading a steel ball with a 10-mm diameter (D, see Figure 8b) to indent the specimen. The Brinell Harness Number (BHN) is the ratio of the load W on the ball to the curved area of the indentation:

$$BHN = \frac{2W}{\pi D^2 \cdot \left[1 - \sqrt{1 - \left(\frac{d}{D}\right)^2}\right]} \qquad (Kg/mm^2) \tag{2}$$

3. The Meyer Hardness number (MHN) is also obtained by indenting a surface with a steel ball, but here the load is divided by the projected area of the indentation $\pi \cdot d^2/4$ on the plane of the specimen surface. This quantity represents the average pressure p, between indenter and specimen, which Meyer proposed as the measure of hardness:

$$MHN = \frac{4W}{\pi \cdot d^2} = p \qquad (Kg/mm^2) \tag{3}$$

where d is the diameter of the projection. From geometrical considerations, a relationship between the Meyer and the Brinell hardness can be obtained:

$$\frac{MHN}{BHN} = \left[1 + \frac{1}{4} \left(\frac{d}{D} \right)^2 \right] = \frac{p}{BHN} \tag{4}$$

The ratio d/D can also be expressed in terms of the BHN:

$$\left(\frac{d}{D} \right)^2 = \frac{4}{\pi} \cdot \frac{W}{D^2} \cdot \left(\frac{1}{BHN} - \frac{W}{\pi \cdot D^2} \cdot \frac{1}{BHN^2} \right) \tag{5}$$

In a hardness test where the depth of penetration h is kept constant, the load W is directly proportional to p. If, on the other hand, W is kept constant, h is proportional to 1/p, so that h decreases with increasing hardness. In the Rockwell test, the value of h is not recorded, only the quantity R_C, as defined in Eq. (1). The relationship between R_C and the BHN for our hardness range for steel is given empirically (ref 10)

$$R_C = c_1 - \frac{c_2}{BHN} \tag{6}$$

where $c_1 = 77.1$ and $c_2 = 13927$ (Kg/mm^2).

Using Eqs. (4), (5), and (6), it is possible to define a relationship between R_C and the mean pressure p

$$b_1 \cdot R_C^2 + (b_2 \cdot p - b_3) \cdot R_C + b_4 - b_5 \cdot p = 0 \tag{7}$$

where the coefficients b_i , i=1...5 are known.

Analysis

Our analysis for the evaluation of the mean pressure p under a spherical indenter for a proper hardness test is based on Figure 8a, as discussed above. In a proper hardness test, the applied load is appropriate to the size of the indenter and to the hardness of the material.

We show here that if residual stresses are present in the plane of the specimen to which the spherical indenter is applied, the pressure p at which plastic deformation starts is changed. The effect of residual stresses on hardness is maximum when plastic deformation starts and the stresses are perpendicular to the pressure induced by the indenter (point A in Figure 8b). This means that as the indenter penetrates further into the specimen, the influence of the residual stresses decreases. We are interested in the average pressure p under the ball and in the average residual stresses σ_H and σ_R. In our calculations, the coefficient α was introduced such that

$$\langle \sigma \rangle = \alpha \cdot \sigma \tag{8}$$

In the following equations, the average brackets are neglected.

Intuitively, one could surmise that if such stresses were present, then in general, the indentation forces would increase or decrease if the stresses were compressive or tensile, respectively. However, this is not true for indentation loads which only cause elastic strains, from the theory of superposition in the

elastic region. The load to generate a certain elastic strain is not affected by stresses in the plane of the specimen. For the plastic region, this is not true, as we shall see.

The problem of deducing mathematical relations to predict the conditions at which plastic deformations begin for stresses in two or three dimensions is a very important consideration in the field of plasticity. The yielding criteria are essentially empirical relationships for predicting the condition at which the material will undergo plastic deformation under a particular combination of stresses. Two yielding criteria are used:

1. The von Mises-Hencky criterion. Yielding occurs at any point in the body when the distortion energy per unit volume for a state of combined stress equals that associated with yielding in a simple tension test ($2\,Y^2$). For principal stresses, as given in Figure 8a, the criterion can be expressed as follows:

$$(\sigma_H - \sigma_R)^2 + \left(-\frac{2}{3}p + \sigma_R + p\right)^2 + \left(-p + \frac{2}{3}p - \sigma_H\right)^2 = 2Y^2 \qquad (9)$$

Solving for p, we denote the pressure as $p_{V\text{-}M}$ for the von Mises-Hencky criterion

$$p_{V\text{-}M} = -\frac{3}{2}(\sigma_H + \sigma_R) + 3\left[Y^2 - \frac{3}{4}(\sigma_H - \sigma_R)^2\right]^{1/2} \qquad (10)$$

2. The Tresca criterion. This assumes that yielding occurs when the maximum shear stress τ_{max} reaches the value Y/2. This can be expressed as

$$\tau_{max} = \frac{(\sigma_1 - \sigma_3)}{2} = \frac{Y}{2} \qquad (11)$$

where σ_1 and σ_3 represent the most tensile and most compressive of the three principal stresses, respectively.

The maximum shear-stress criterion of Tresca is less complicated mathematically than the von Mises-Hencky criterion, and for this reason, it is often used in engineering design. However, in our case, in order to achieve a correlation between the experimental hardness and residual stress data, we had to neglect the effect of radial stress σ_R. In the case in which σ_R is algebraically larger than σ_H, this assumption is not valid, and results from this analysis are not correct within the Tresca framework. In using the Tresca criterion, we should write

$$\tau_{max} = \frac{1}{2}\left[-\frac{2}{3}P + \max(\sigma_H, \sigma_R) + P\right] = \frac{Y}{2} \qquad (12)$$

Since we neglected the presence of radial stress in the calculations involving the Tresca criterion, the following relationship was used for the pressure denoted as $p_{P\text{-}T}$

$$\mu_{P\text{-}T} = 3\cdot(Y - \sigma_H) \tag{13}$$

where the subscript P-T stands for Pseudo-Tresca, since this is an approximation of the Tresca yielding criterion.

Equations (10) and (13) represent the model's predicted pressure at which deformation takes place at point A in Figure 8b just below the indenter. Here the pressure p and the residual stresses are perpendicular, but this is not the same across the whole surface of the indentation. For this reason, the parameter α was introduced in Eq. (8), and the average stresses are substituted in Eqs. (10) and (13).

FIT OF EXPERIMENTAL DATA

Equations (10) and (13) describe the relationship between the average pressure, the yield strength, and the residual stress of the material. These relationships were incorporated into Eq. (7) to obtain the model's final expression for the predicted R_C. The only unknowns in the final expression of R_C are the yield strength and the coefficient α. The principal effect of the yield strength is to modify the value of the zero residual stress hardness R_{Co}, while α represents the effect of the non-perpendicularity of the residual stresses to the pressure p applied by the indenter.

The general linear least squares algorithm was used to fit the set of hardness data points to the model proposed above. For this purpose, the merit function χ^2 was defined as follows:

$$\chi^2(Y, \alpha) = \sum_{i=1}^{N}\left(\frac{R_X(x_i) - R_C[x_i;\ Y, \alpha]}{\sigma_i(x_i)}\right)^2 \tag{14}$$

where $R_X(x_i)$ *is* R_C *experimentally measured at position* x_i, R_C *is the predicted* value, and σ_i is the standard deviation of the experimental data.

The purpose of our procedure was to evaluate yield strength and coefficient α, which minimize the function χ^2. The Downhill Simplex Method was utilized (ref 11). The method requires only function evaluations, therefore, it is not efficient in terms of the number of iterations required. However, it does have the advantage of not having to evaluate the derivatives.

Results for the fitted parameters are given in Table 1, where R_{Co} is obtained from Eq. (7).

Table 1. Summary of Results For Two Yield Criteria
Y and α are variable

Sample	Method	α	Y (Kbar)	R_{Co}	χ^2
100%	V-M	0.160	12.10	38.5	0.016
FC6355	V-M	0.180	12.14	38.6	0.014
G	V-M	0.210	12.94	41.1	0.044
100%	P-T	0.083	12.16	38.7	0.016
FC6355	P-T	0.090	12.16	38.7	0.022
G	P-T	0.107	13.02	41.3	0.099

A rule of thumb for estimating the "goodness" of fit is to compare the value of χ^2 for different fits. It is clear that the von Mises-Hencky criterion is a better fit to the experimental data than the Pseudo-Tresca criterion, especially in the case of sample G. In this fit, the parameter α decreases as the yield strength of the material decreases. This was expected in terms of our understanding of the phenomenon. As previously stated, the effect of residual stress diminishes as the indenter penetrates more into the material, and the plastic deformation region increases in size. The fact that the coefficient α for the von Mises' case is twice that for the Pseudo-Tresca case, can be understood by the nature of the two different yielding criteria. In simplifying the von Mises expression, a factor of one-half multiplies the residual stress.

To make this model useful for characterizing residual stresses using hardness measurements, we considered the case where α is constant. Hence, the model could be used at least in the range of Y, which appeared in our specimen. A second fit was performed using a fixed value for α. For von Mises, we assumed $\alpha = 0.18$ and for Pseudo-Tresca, we assumed $\alpha = 0.09$. The results are given in Table 2.

Table 2. Summary of Results For Two Yield Criteria
Y is variable, α is fixed

Sample	Method	α	Y (Kbar)	R_{Co}	χ^2
100%	V-M	0.18	12.14	38.6	0.020
FC6355	V-M	0.18	12.14	38.6	0.014
G	V-M	0.18	12.95	41.1	0.082
100%	P-T	0.09	12.16	38.7	0.019
FC6355	P-T	0.09	12.16	38.7	0.022
G	P-T	0.09	13.02	41.0	0.149

The fitted values of the hardness versus the residual hoop stress are plotted in Figures 9, 10, and 11. Also plotted in Figure 9 is the result of the fit obtained using the complete Tresca criterion. The agreement is clear in the tension region of the hoop stress ($\sigma_H > \sigma_R$), but in the region ($\sigma_H < \sigma_R$), the agreement is poor.

In the case of sample G, the residual stresses present are higher and reach a value comparable to more than one-half of the yield strength of the material at the ID. The related hardness does not increase linearly in this range of values. This explains the better fit obtained by the von Mises-Hencky model in the case of sample G. This sample is also slightly harder than the others, resulting in a higher value of R_{Co}.

The model satisfactorily represents the relationship between measured values of residual stress and hardness. The larger disagreement between experimental and calculated data occurs around the point where the elastic-plastic transition due to autofrettage occurs. In the case of measured stress data, the transition is very sharp, and this point can be accurately measured. In the case of hardness data, this transition is muted, as if an average measurement were performed. As a result, the measurement in this region is not precise. As we go away from this point, the fit is very good, as shown in sample FC6355. Again, for sample G, we were not able to improve the fit. Results of the fit are shown in Figures 12, 13, and 14, where the experimentally measured hardness versus position is plotted together with the calculated values obtained using both the Pseudo-Tresca and von Mises-Hencky criteria. The parameters used in this case are shown in Table 2. The fit can be considered "good" in the regions distant from the plastic-elastic transition due to autofrettage, but they are not consistent near the transition point.

The relationship between R_C and hoop residual stress is depicted in Figure 15 for all three specimens. It shows the consistency of the measurements and the model. The data and model from the two rings manufactured from the same material and with the same heat treatment fall right on top of each other. The R_{C_o} and yield strength resulting from the two are the same. The parameter α reflecting the average effect of the residual stress on yielding is somewhat different, but the model does not require them to be the same. The curve in this figure for the third ring, G, is also parallel to the data from the first two rings, but reflects a different R_{C_o}. Indeed G, manufactured years earlier, does have a higher hardness than the other two rings. In this case, the similarity of the FC6355 and 100 percent fits can be used to refute the possibility that there is a relationship between the amount of plastic strain and hardness that one may find for annealed or mild steels. These two rings had different amounts of autofrettage and consequently, different amounts of plastic strain. In spite of that, our model using the von Mises-Hencky yielding criterion, including only residual stress effects, consistently fits the data. This data does not show any greater deviation from the model in the regions that were heavily plastically deformed.

To further investigate the possibility that plastic deformation caused systematic changes in the hardness, we cut a one-inch pie-shaped wedge from a ring adjacent to specimen FC6355 to release the stresses caused by the autofrettage. We then measured the R_C as a function of radial position in the wedge, as previously done in the ring. We found that the hardness within one-eighth inch of the cut was constant and had the expected value at zero stress for FC6355 equal to R_{C_o} in Table 1. As we measured the hardness further away from the cut surface, we did not find constant R_C, but that the hardness fluctuated with position along the radius and differed from the hardness values shown in the uncut ring or near the edge. We conclude that for the pie-shaped specimen, there is a greater tendency for the microstresses associated with the intergranular stresses to relax nearest the cut, very close to the edge of the specimen. Further into the body of the specimen, these stresses between grains persist, corrupting the hardness measurements, even though the long range stresses are relaxed. It is plausible that one component of the dependence of hardness values on strain history or amount of strain hardening of the material is due to the plastic deformation associated with the straining that leaves intragranular stresses in the material. For the specimens FC6355 and 100 percent, although these intragranular stresses can add scatter to the R_C, they would not affect them systematically. For specimen G, the difference between the model and the experimental data is the greatest, approximately one in the R_C scale, near the O.D., i.e., on the tension side of the residual stress. This also causes a little tail for the calibration curve shown in Figure 15. This could be attributed to the possibility of high axial stresses in specimen G, which is the thickest of all the specimens, and may have distorted the hoop stress distribution in the cylinder. The axial stresses result from autofrettage by an oversized mandrel pushed through the tube. As the plastic deformation proceeds by this method, axial stresses are also introduced; these stresses exist in the tube and are relieved more in thinner rings when the tube is cut than in thicker rings. Unlike the other two, specimen G may also be subject to the effect that different amounts of plastic strain can cause strain hardening and therefore affect the R_C hardness in addition to the amount of residual stress.

CONCLUSIONS

A model was presented to evaluate the effect of residual stress on the measured Rockwell C hardness. The model satisfactorily fits experimental hardness versus residual stress data obtained for three tubes with different percentages of autofrettage over a hardness range R_C 37 to 43 for the three rings. The calibration and fit for the three specimens is consistent. The model gives the same yield strength (175 Ksi) for two specimens of the same material but different amounts of autofrettage. The von Mises-Hencky yield criterion seems to provide a better fit to the data than the Tresca criterion.

The results of this model, namely the necessity for introducing a fitting parameter α as explained in the text, are corroborated by the results of Blain (ref 2) who used a ball indentation test in steel only to the very onset of plastic deformation to detect surface residual stress. He found a much larger change in the load required to produce the onset of plastic deformation as a function of compressive or tensile

surface residual stress than in R_C for the same range of residual stress. This leads us to further investigate the possibility of a more efficient test for surface residual stresses that can be understood within this model. Even at this time, this model and this set of experiments with proper calibration for a given type of steel can be used as a basis for the measurement of surface residual stress in steels.

REFERENCES

1. E. Holm, R. Holm, and E.I. Shobert II, "Theory of Hardness and Measurements Applicable to Contact Problems," *Journal of Applied Physics*, Vol. 20, April 1949, pp. 319-320.

2. P.A. Blain, "Influence of Residual Stress on Hardness," *Metal Progress*, Vol. 71, 1957, pp. 96-100.

3. G.U. Oppel, "Biaxial Elasto-Plastic Analysis of Load and Residual Stresses," *Experimental Mechanics*, Vol. 4, No. 5, 1964, pp. 135-140.

4. T.R. Sines, S.G. Mellor, and D.A. Hills, "A Note on the Influence of Residual Stress on Measured Hardness," *Journal of Strain Analysis*, Vol. 19. No. 2, 1984, pp. 135-137.

5. B.B. Brown, "Measurement of the Extent of Autofrettage in Tube Sections," Technical Report ARLCB-TR-83042, Benet Weapons Laboratory, Watervliet, NY, December 1983.

6. J. Frankel, W. Scholz, G. Capsimalis, and W. Korman, "Residual Stress Measurement in Circular Steel Cylinders," *Proceedings of IEEE Ultrasonic Symposium*, 1983, pp. 1009-1012.

7. W. Scholz and J. Frankel, "Acoustoelastic Effects in Autofrettaged Steel Cylinders," *Proceedings of Conf. Ultrasonics International*, Butterworth & Co. Publ. Ltd., 1985, pp. 441-446.

8. J.A. Kapp and G.A. Pflegl, "Stress Analysis of O.D. Notched Thick-Walled Cylinders Subjected to Internal Pressure With Thermal Loads," *Journal of Pressure Vessel Technology*, Vol. 103, February 1981, pp. 76-81.

9. M.C. Shaw, T. Hoshi, and D. Henry, "Reverse Plastic Flow Associated With Plastic Indentation," *Transactions of the ASME*, Vol. 101, May 1979, pp. 104-108.

10. T. Tabor, *The Hardness of Metals*, Oxford at the Clarendon Press, 1951.

11. W.H. Press, B.P. Flannery, S.A. Teukolsky, and W.T. Vetterling, *Numerical Recipes. The Art of Scientific Computing*, Cambridge University Press, 1986, pp. 289-293.

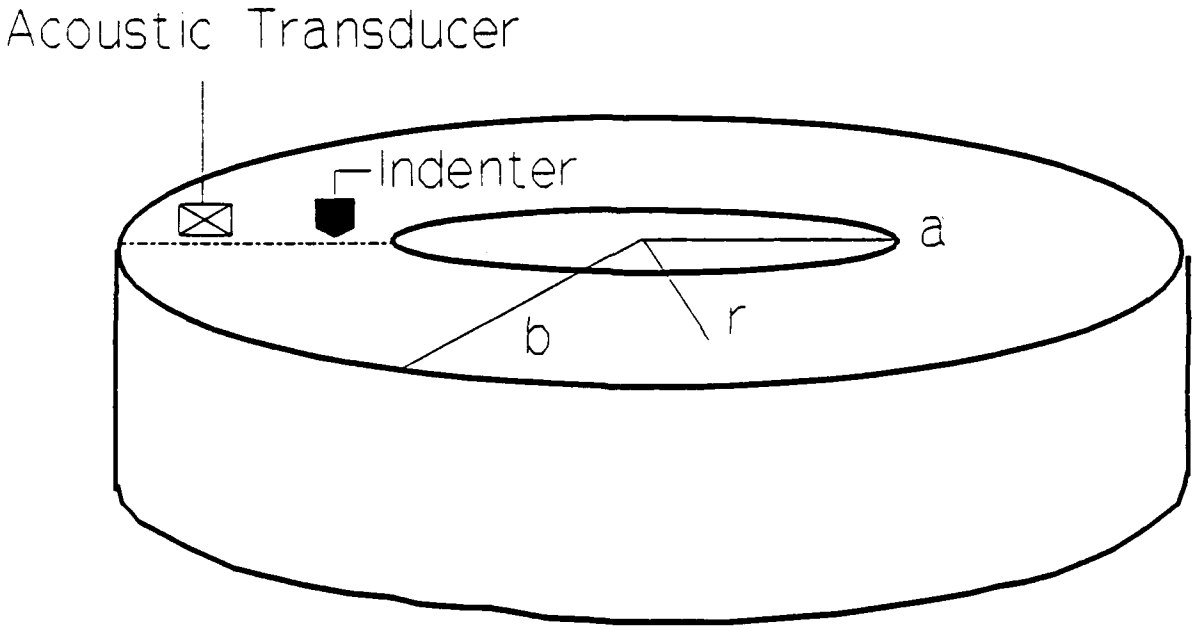

Figure 1. Schematic representation of the gun slice and testing setup used in the experiments.

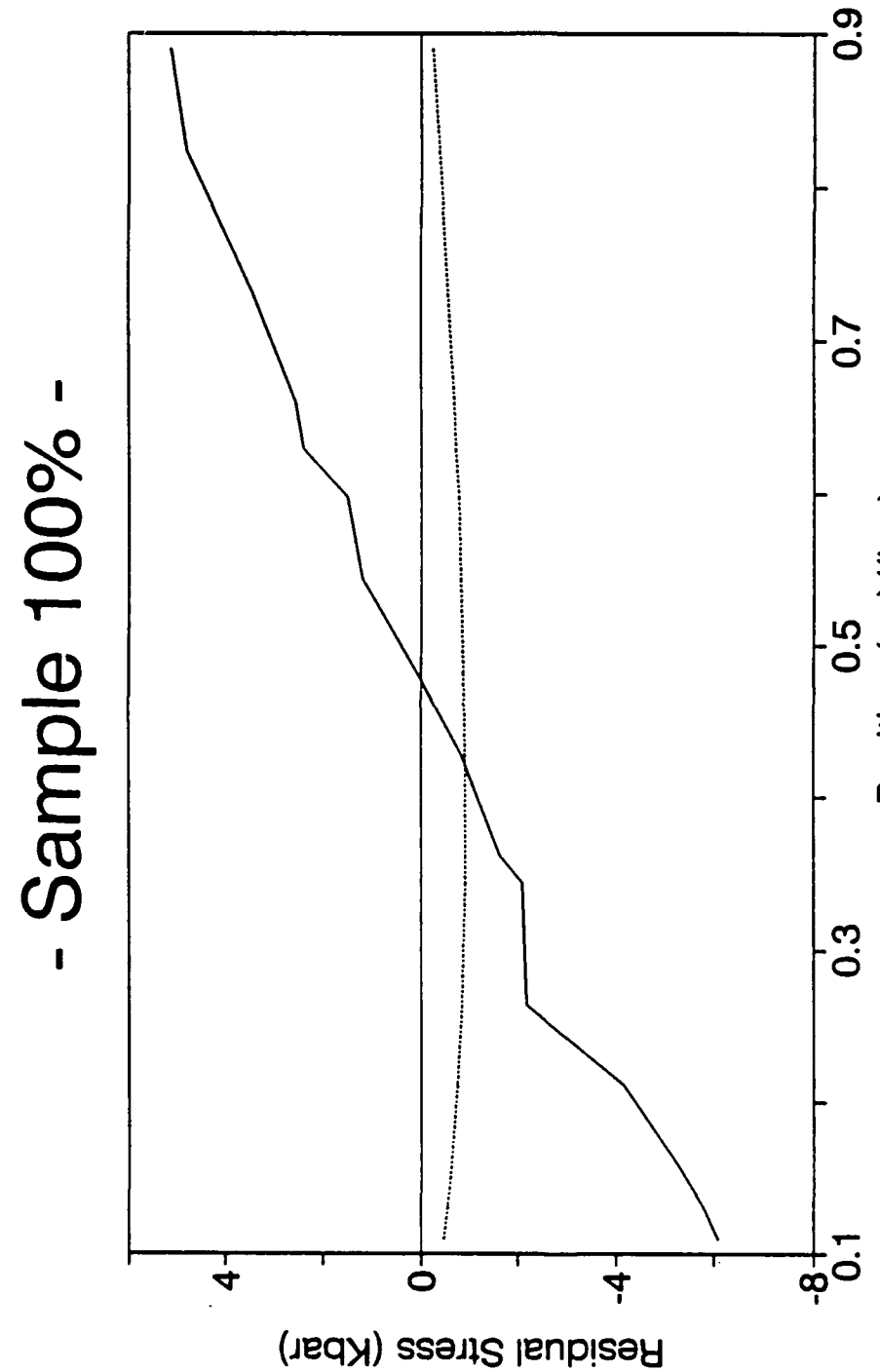

Figure 2. Hoop and radial stress measured for sample 100 percent.

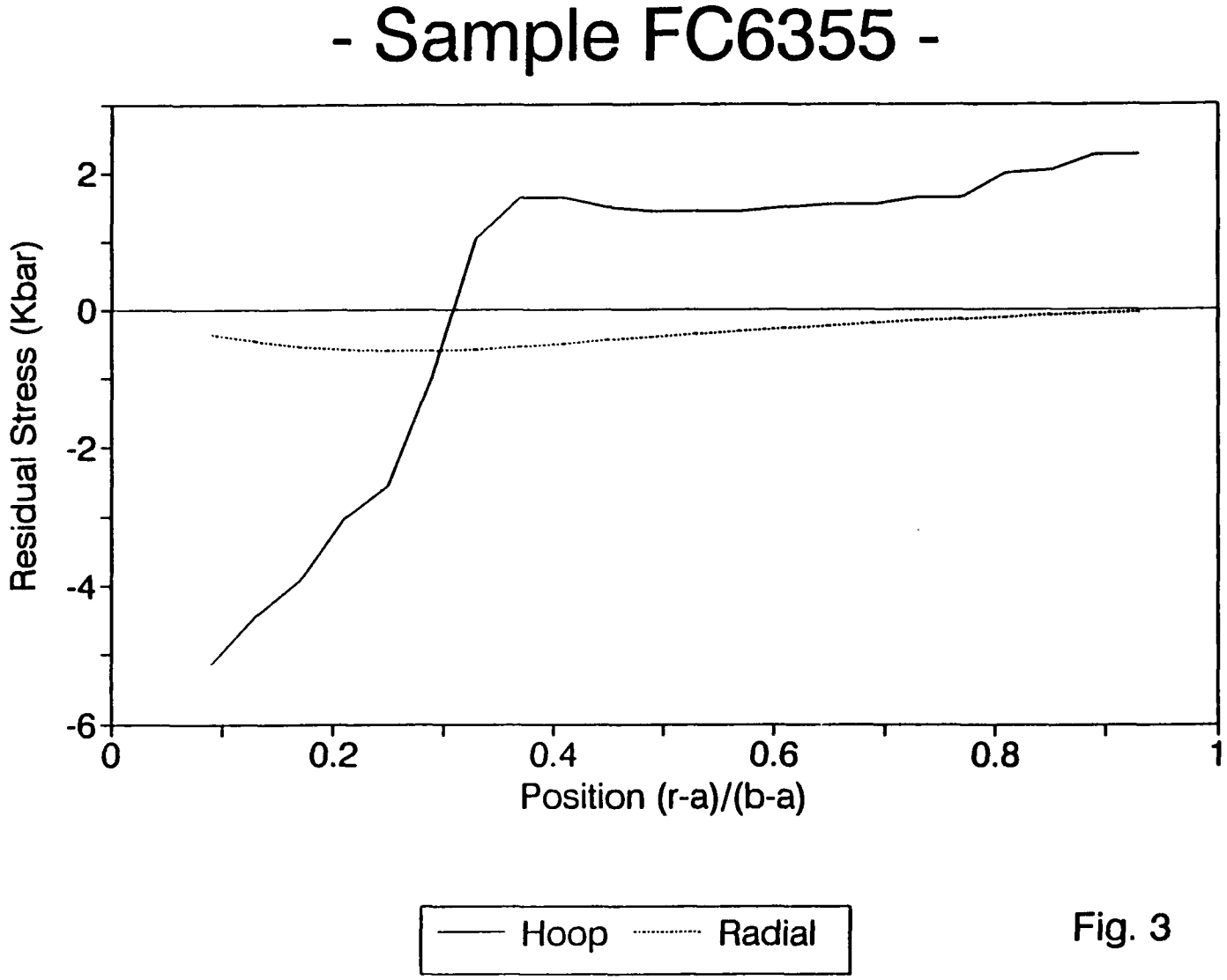

Figure 3. Hoop and radial residual stress measured for sample FC6355.

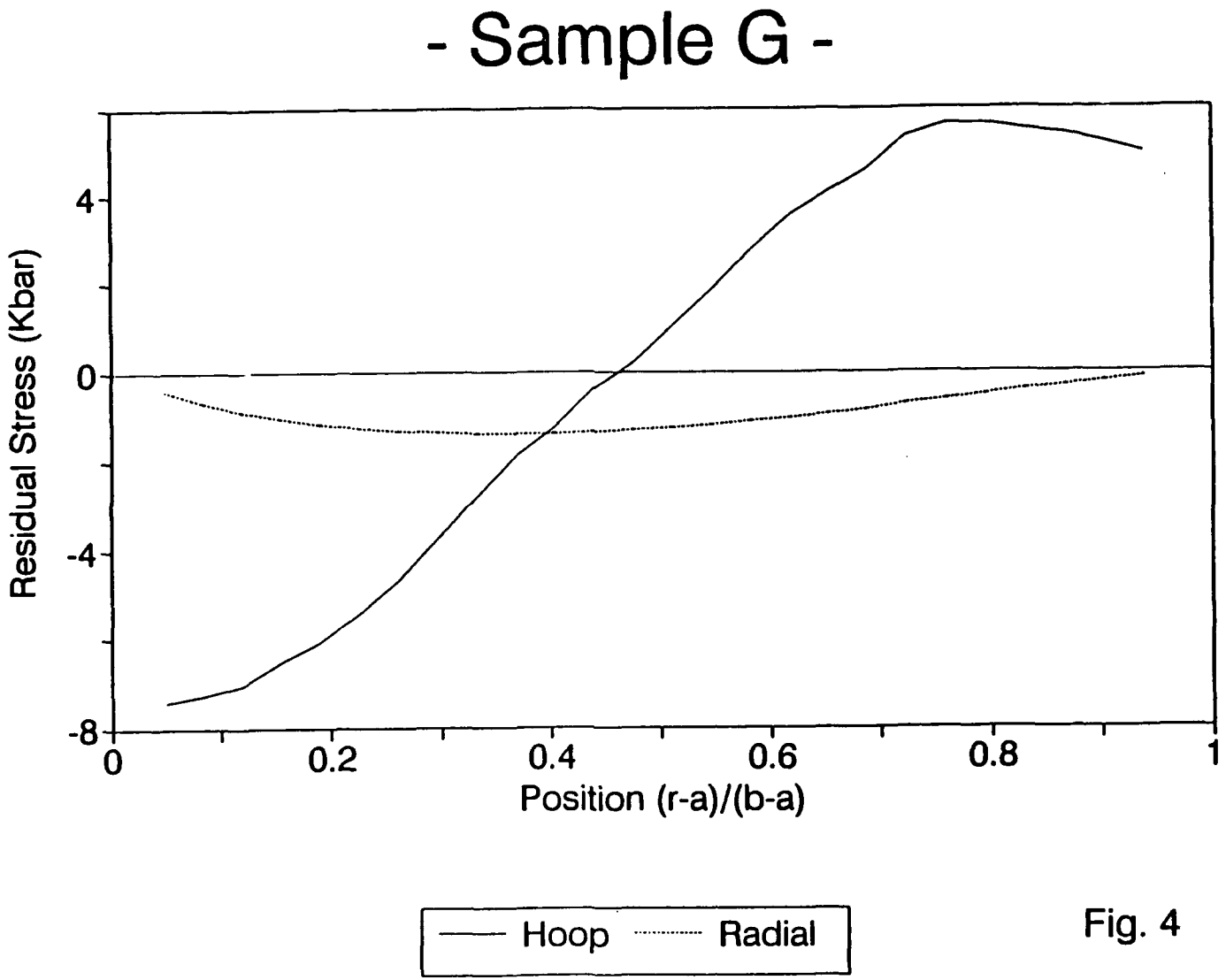

Fig. 4

Figure 4. Hoop and radial residual stress measured for sample G.

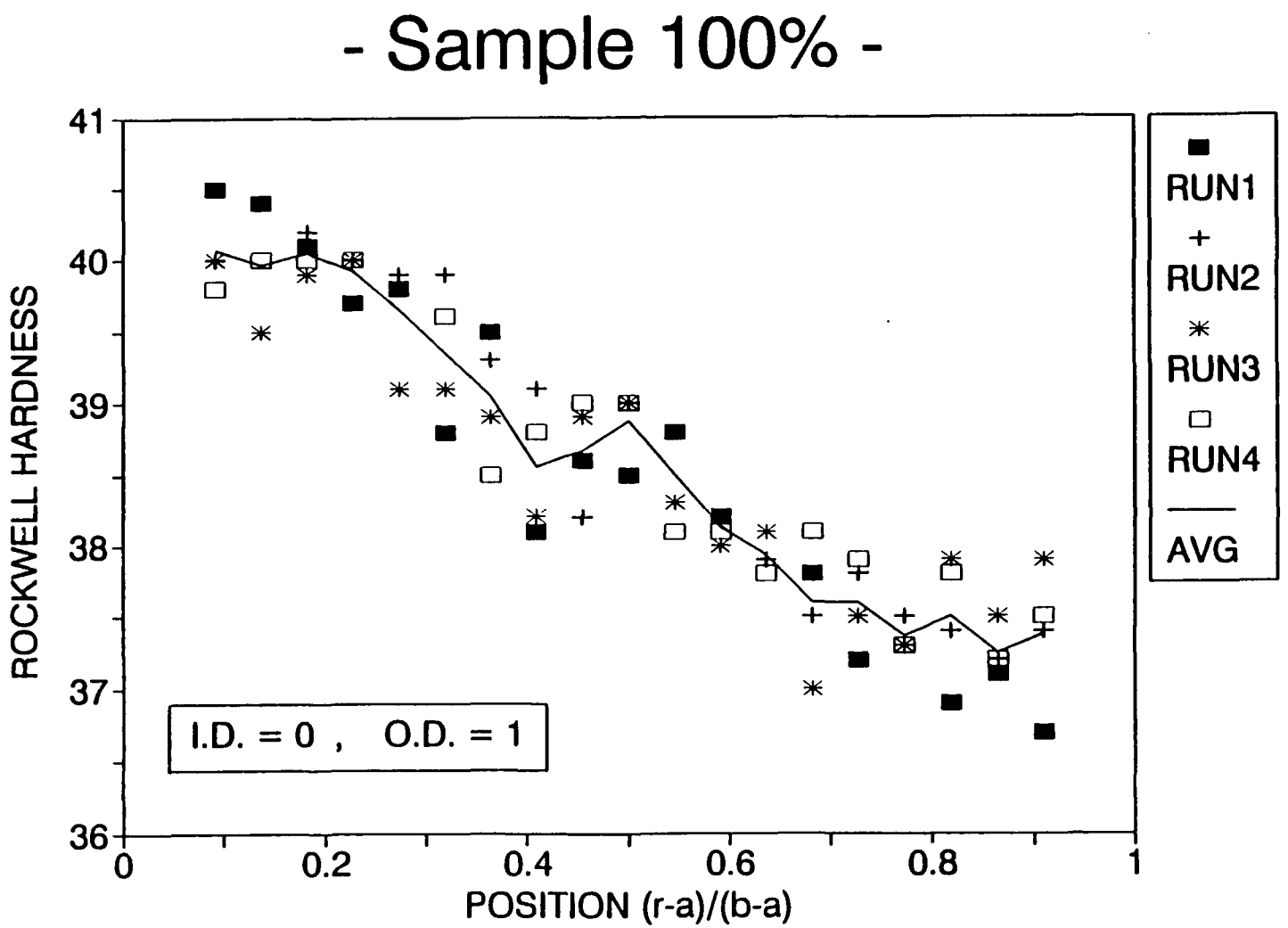

Figure 5. Rockwell C hardness readings for sample 100 percent. The line represents the average of the various readings.

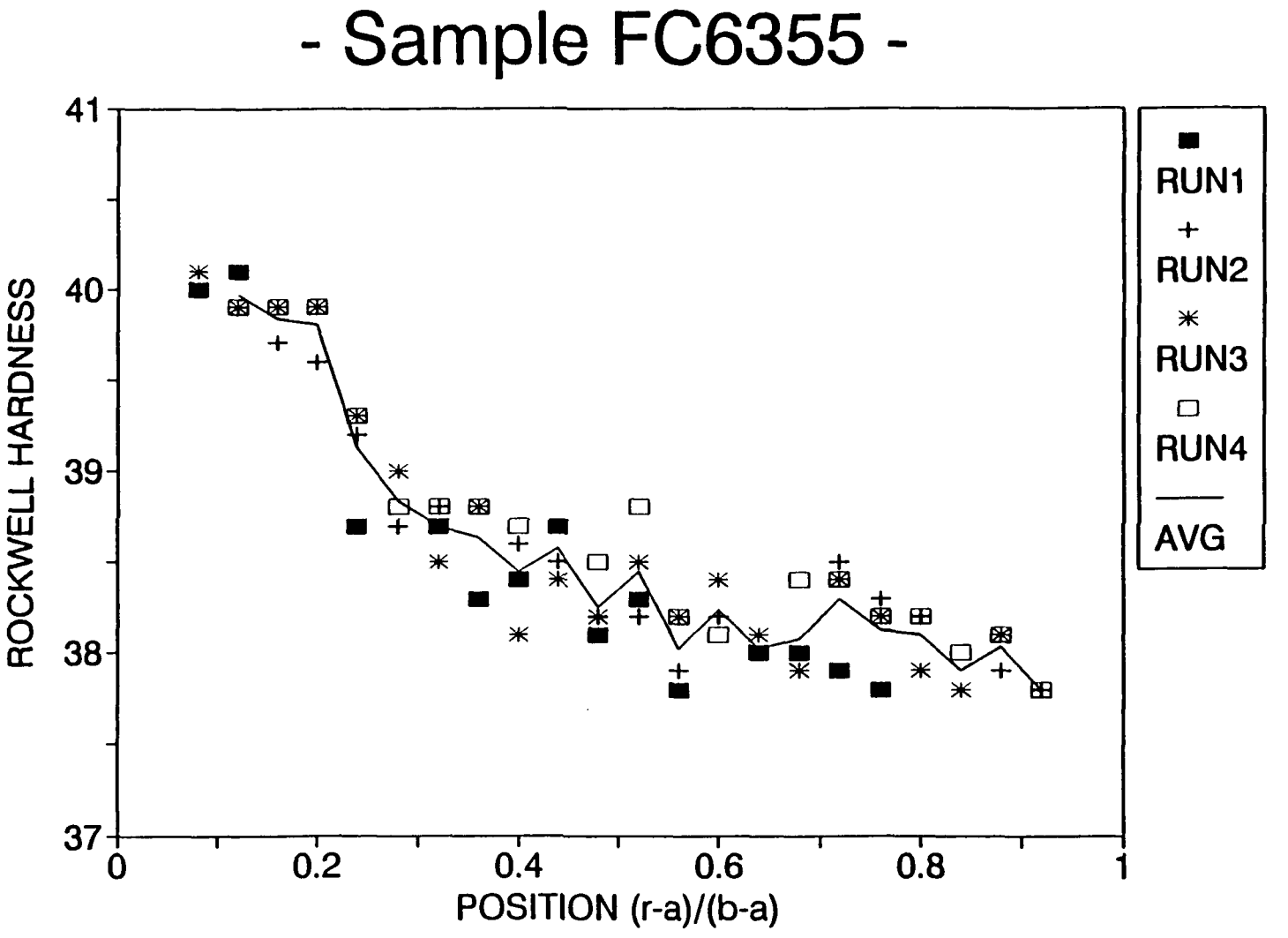

Figure 6. Rockwell C hardness readings for sample FC6355. The line represents the average of the various readings.

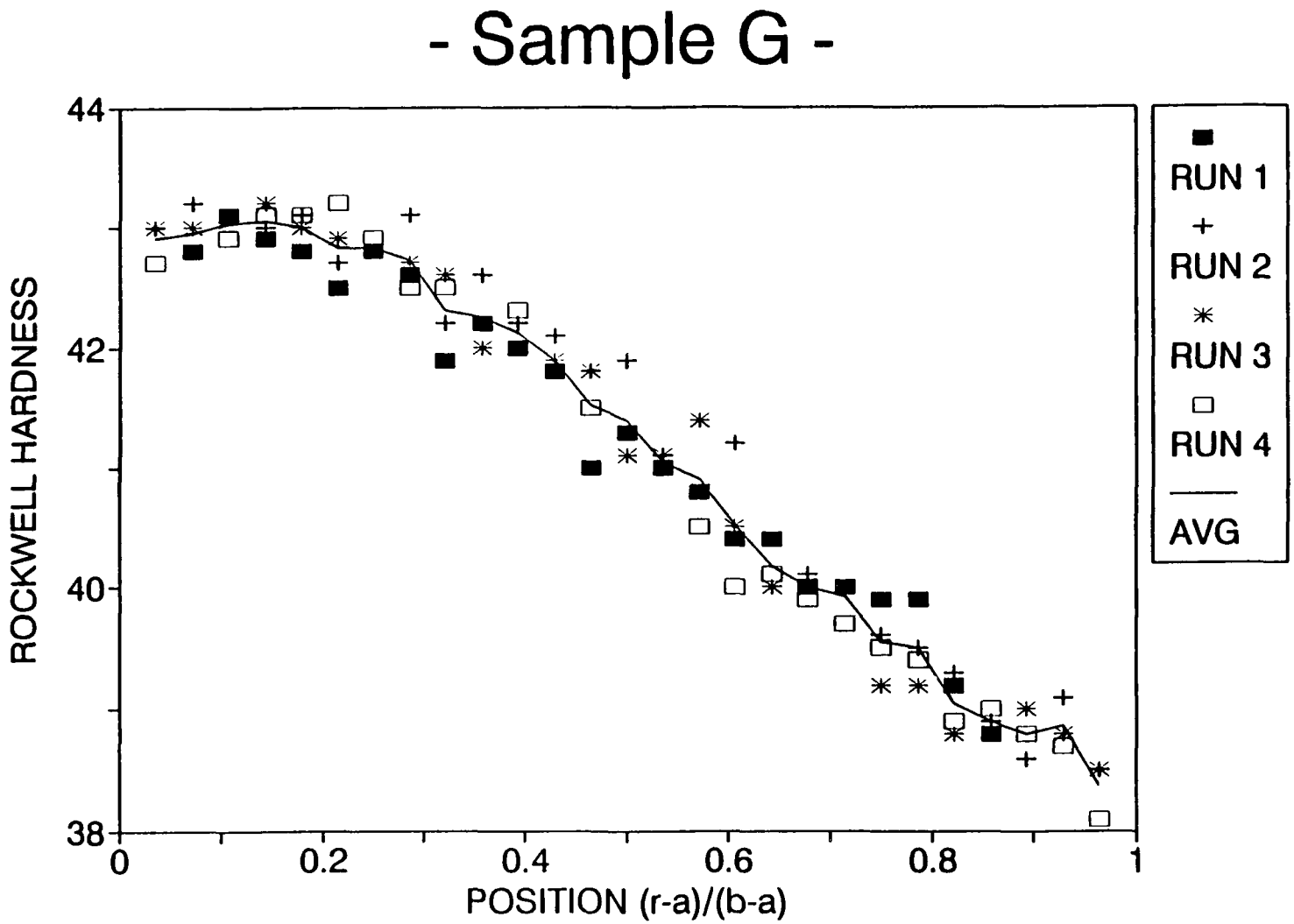

Figure 7. Rockwell C hardness readings for sample G. The line represents the average of the various readings.

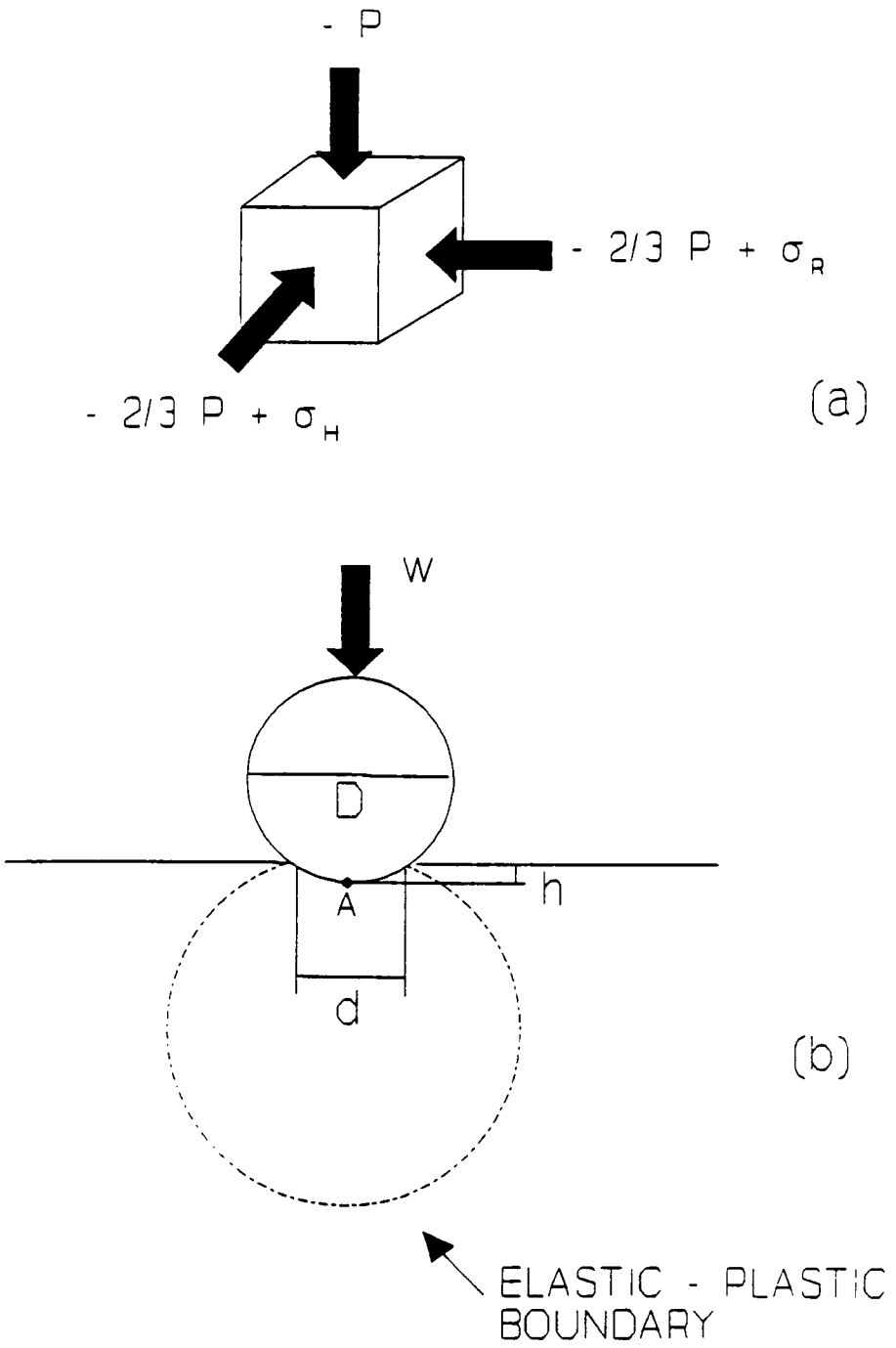

Figure 8. Schematic representation of the stresses below a spherical indenter. The stresses in point A of Figure 8b are represented in Figure 8a.

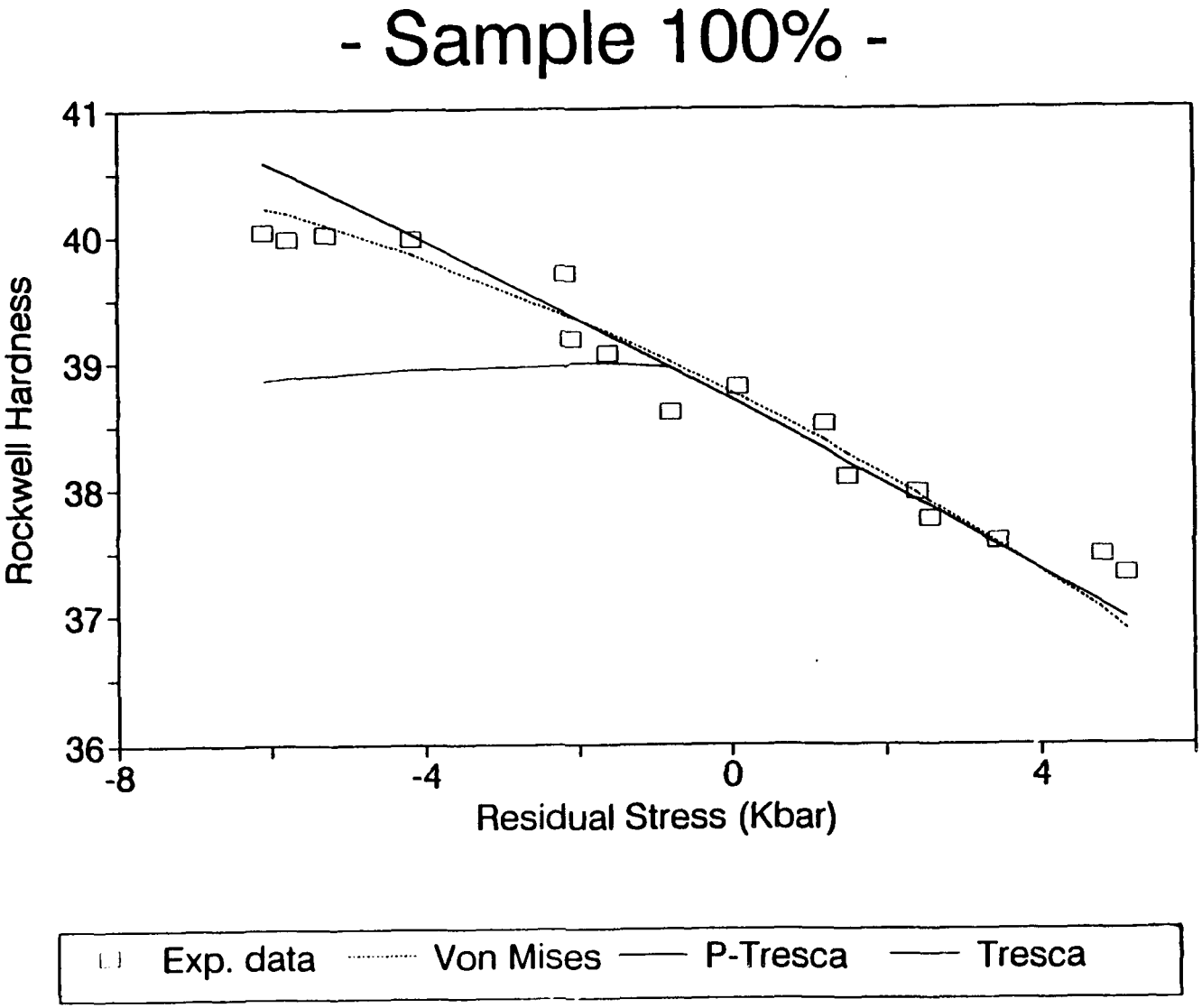

Figure 9. Plot of the Rockwell C hardness as a function of the hoop residual stress for sample 100 percent. The symbols indicate the experimental data while the lines represent the various fits.

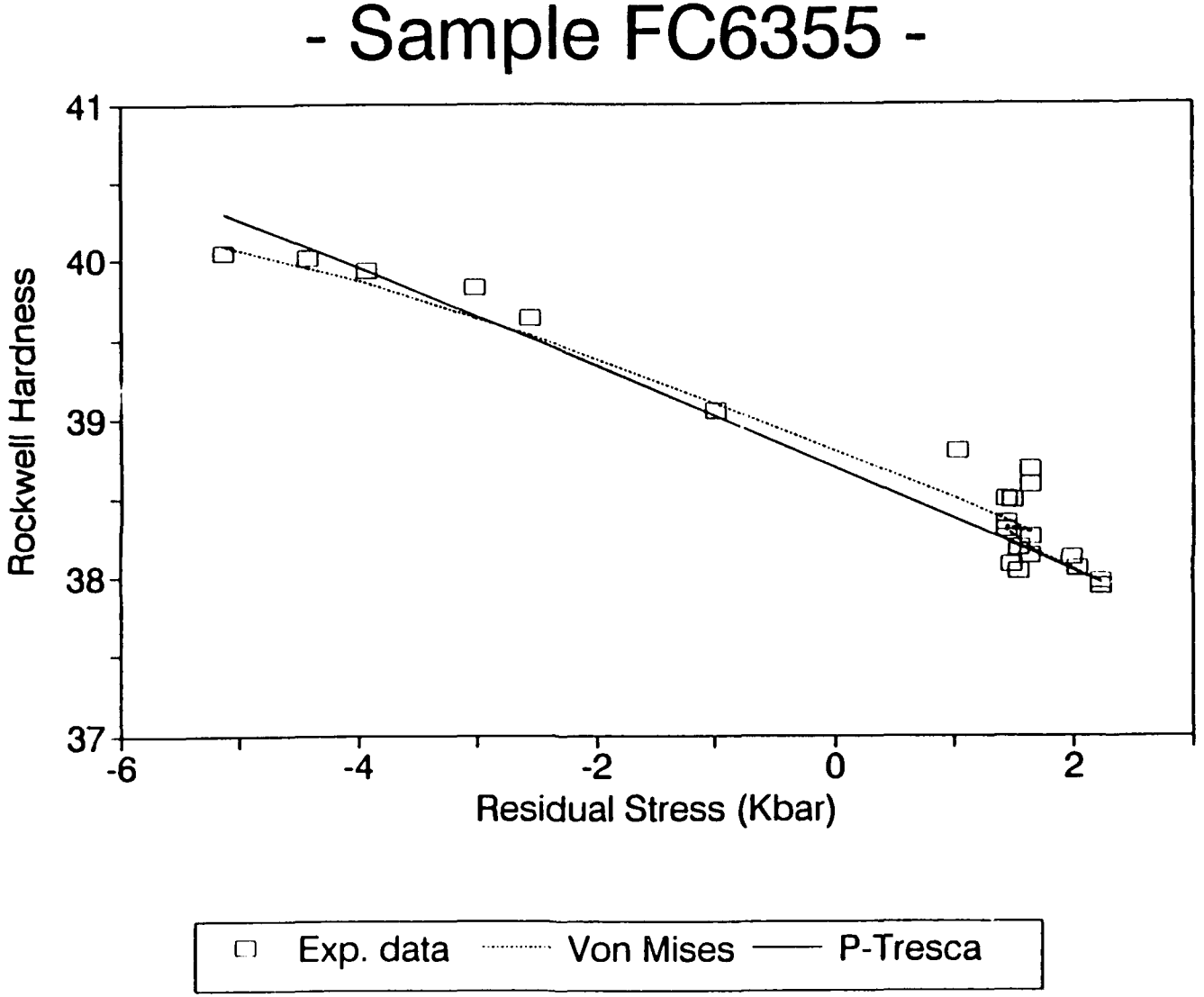

Figure 10. Plot of the Rockwell C hardness as a function of the hoop residual stress for sample FC6355. The symbols indicate the experimental data while the lines represent the various fits.

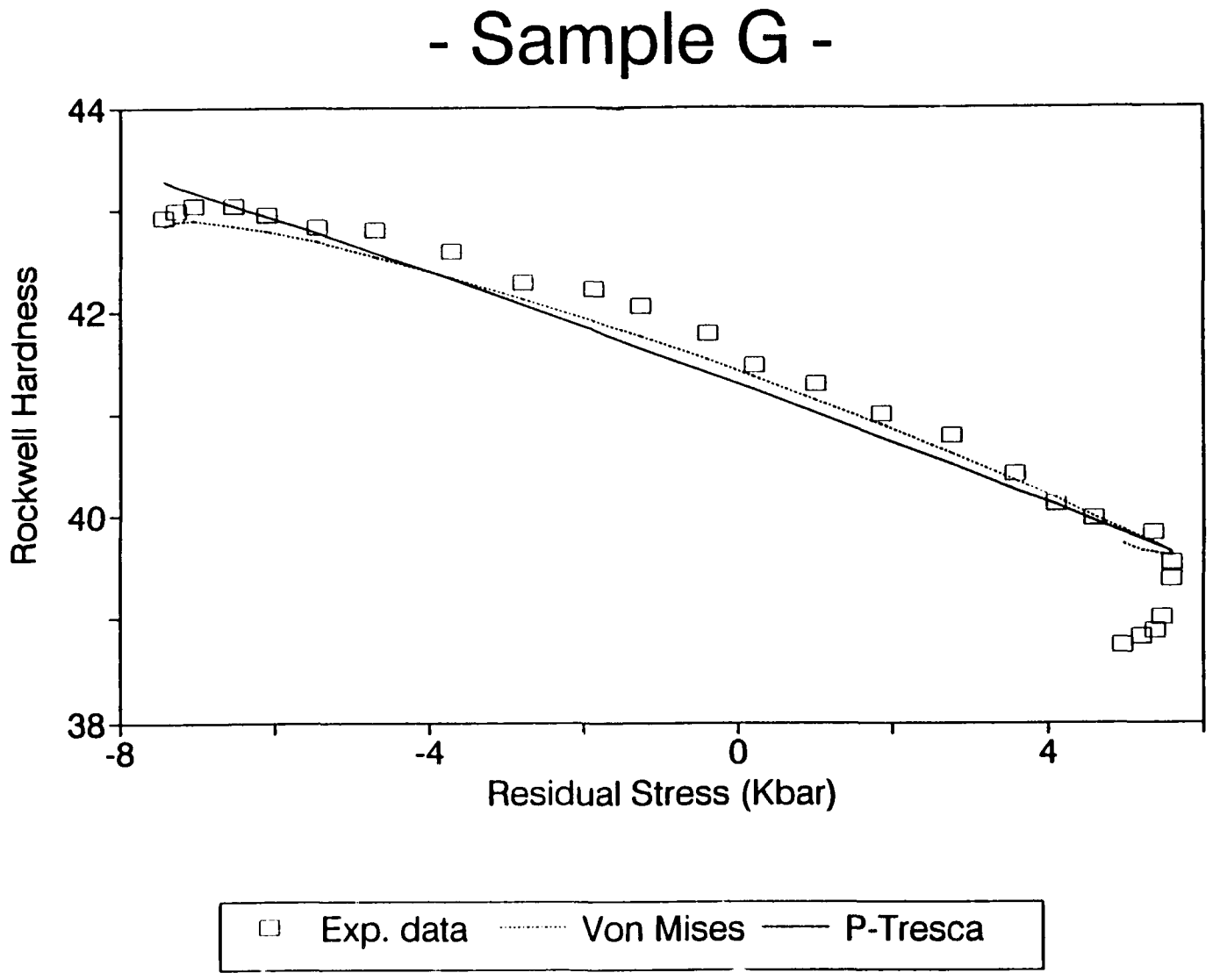

Figure 11. Plot of the Rockwell C hardness as a function of the hoop residual stress for sample G. The symbols indicate the experimental data while the lines represent the various fits.

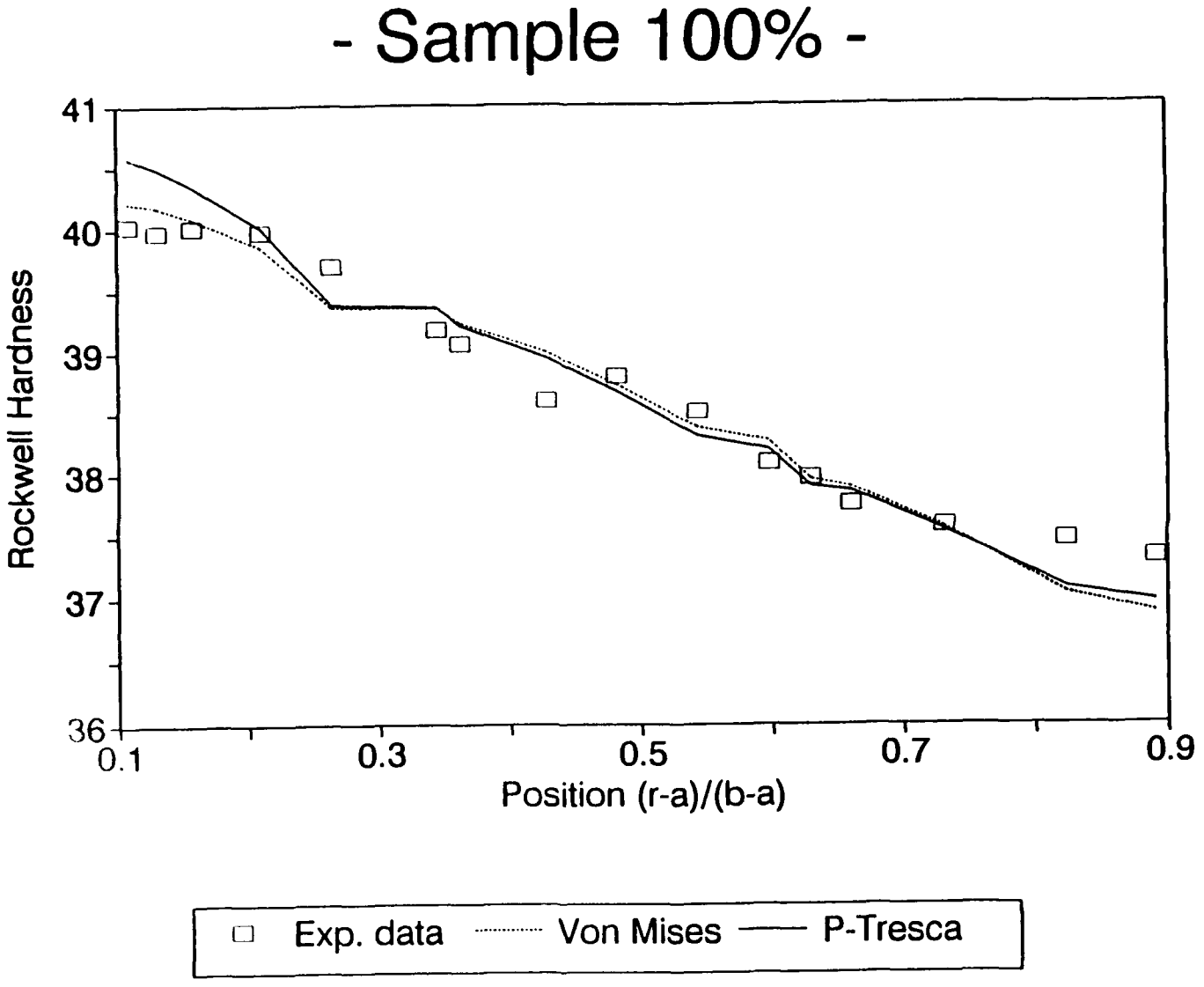

Figure 12. Plot of the Rockwell C hardness as a function of the radial position for sample 100 percent. The symbols indicate the experimental data while the lines represent the various fits.

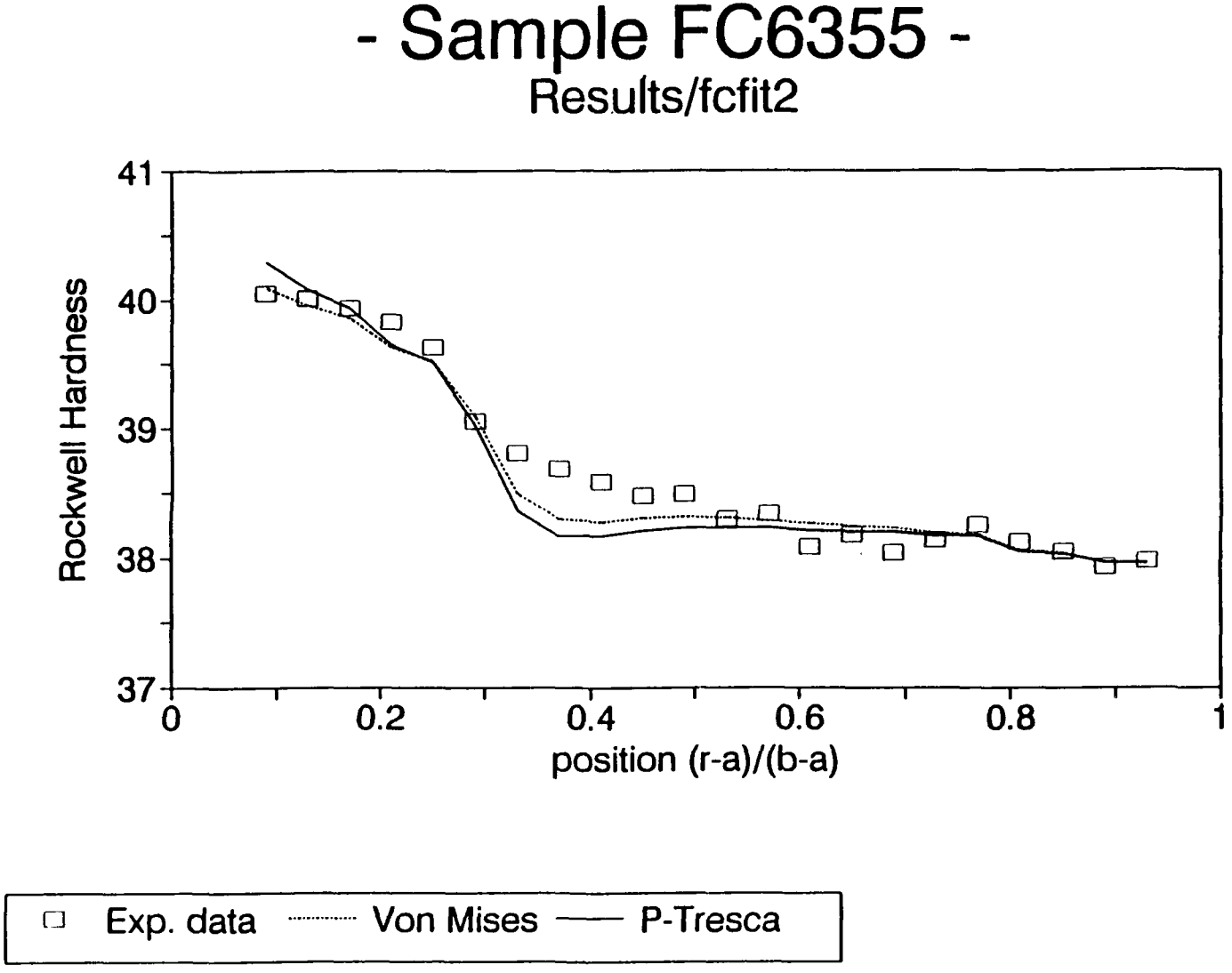

Figure 13. Plot of the Rockwell C hardness as a function of the radial position for sample FC6355. The symbols indicate the experimental data while the lines represent the various fits.

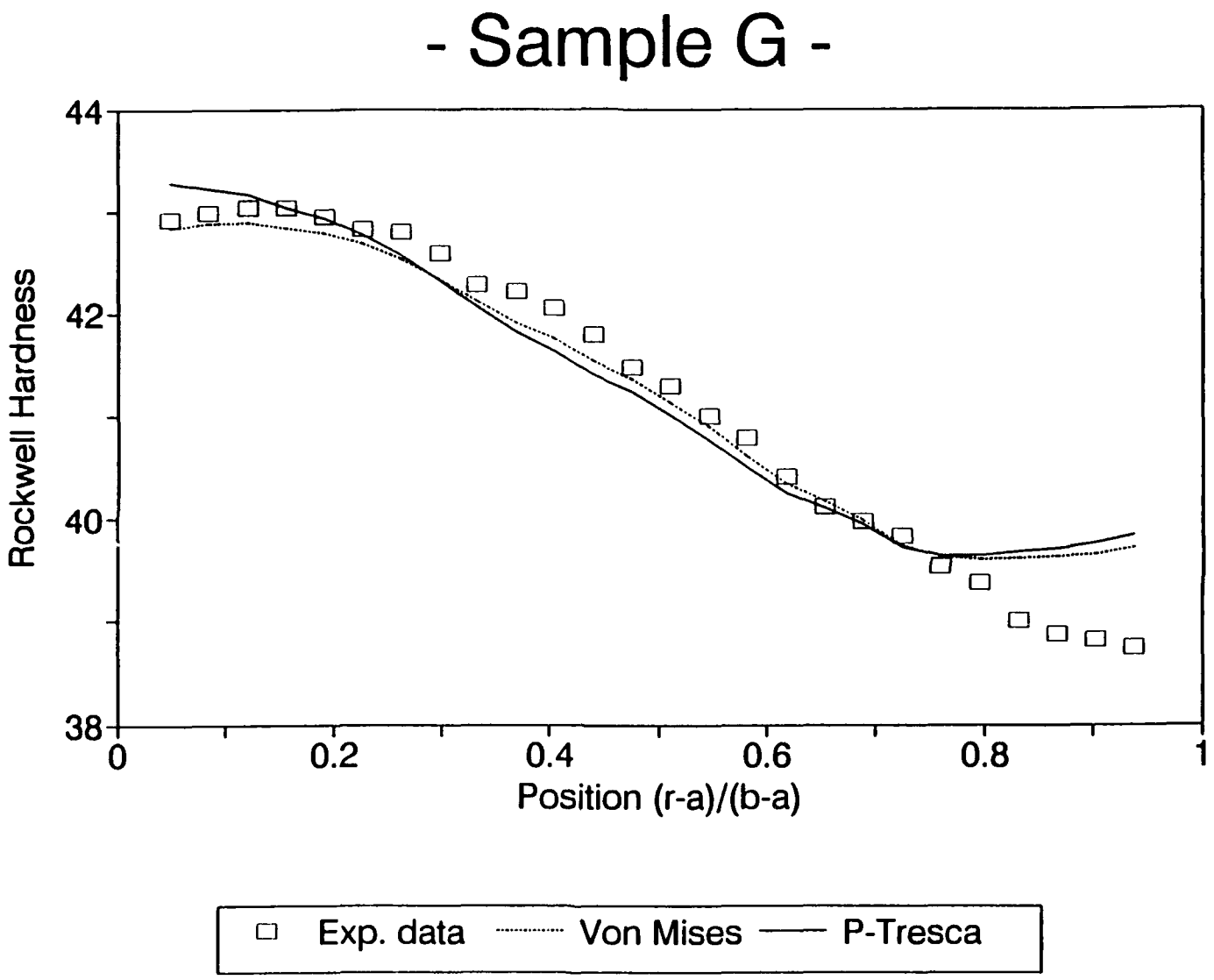

Figure 14. Plot of the Rockwell C hardness as a function of the radial position for sample G. The symbols indicate the experimental data while the lines represent the various fits.

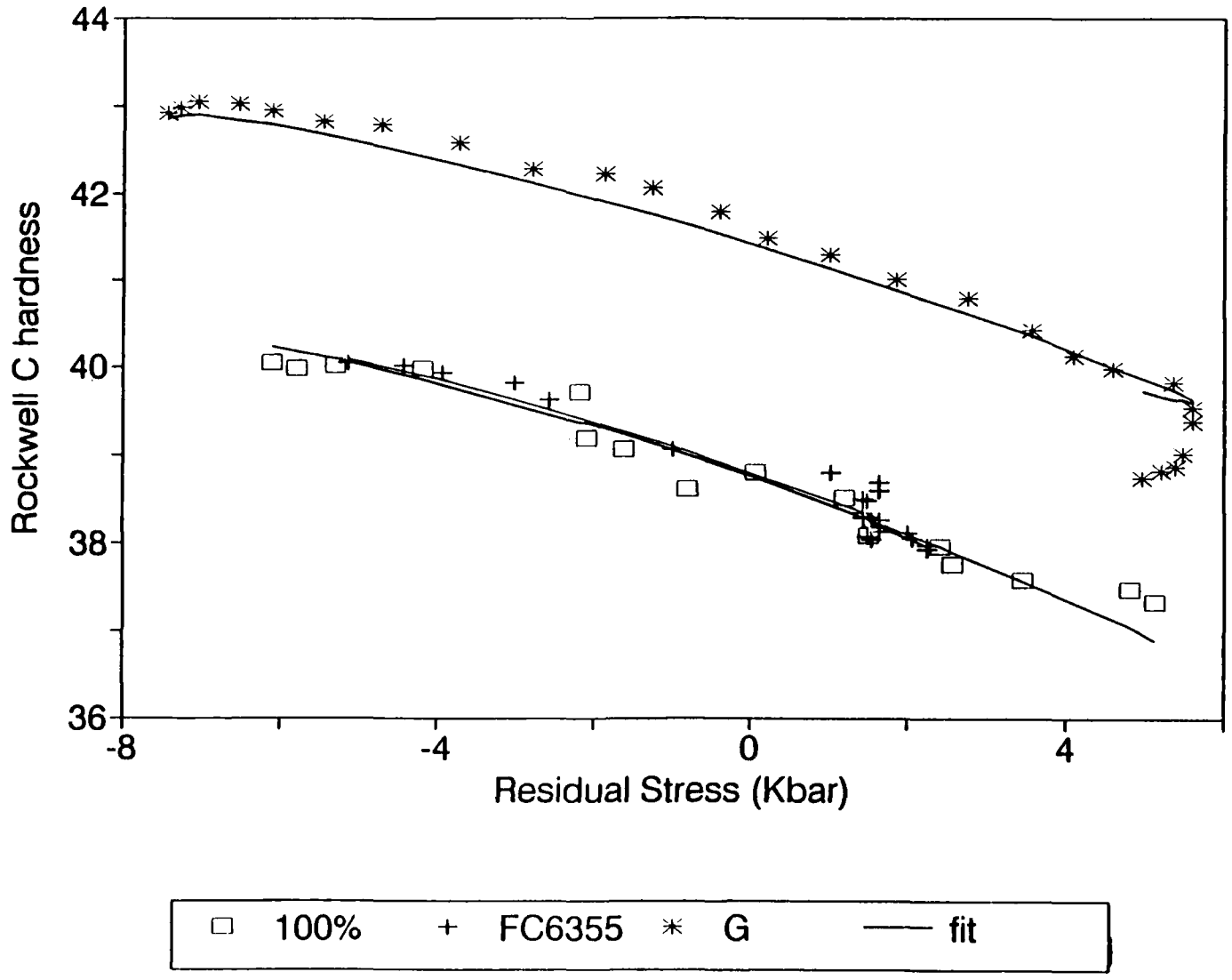

Figure 15. Measured and calculated Rockwell C hardness as a function of the hoop residual stress.

TECHNICAL REPORT INTERNAL DISTRIBUTION LIST

	NO. OF COPIES
CHIEF, DEVELOPMENT ENGINEERING DIVISION	
ATTN: SMCAR-CCB-DA	1
-DC	1
-DI	1
-DR	1
-DS (SYSTEMS)	1
CHIEF, ENGINEERING SUPPORT DIVISION	
ATTN: SMCAR-CCB-S	1
-SD	1
-SE	1
CHIEF, RESEARCH DIVISION	
ATTN: SMCAR-CCB-R	2
-RA	1
-RE	1
-RM	1
-RP	1
-RT	1
TECHNICAL LIBRARY	5
ATTN: SMCAR-CCB-TL	
TECHNICAL PUBLICATIONS & EDITING SECTION	3
ATTN: SMCAR-CCB-TL	
OPERATIONS DIRECTORATE	1
ATTN: SMCWV-ODP-P	
DIRECTOR, PROCUREMENT DIRECTORATE	1
ATTN: SMCWV-PP	
DIRECTOR, PRODUCT ASSURANCE DIRECTORATE	1
ATTN: SMCWV-QA	

NOTE: PLEASE NOTIFY DIRECTOR, BENET LABORATORIES, ATTN: SMCAR-CCB-TL, OF ANY ADDRESS CHANGES.

TECHNICAL REPORT EXTERNAL DISTRIBUTION LIST

	NO. OF COPIES
ASST SEC OF THE ARMY RESEARCH AND DEVELOPMENT ATTN: DEPT FOR SCI AND TECH THE PENTAGON WASHINGTON, D.C. 20310-0103	1
ADMINISTRATOR DEFENSE TECHNICAL INFO CENTER ATTN: DTIC-FDAC CAMERON STATION ALEXANDRIA, VA 22304-6145	12
COMMANDER US ARMY ARDEC ATTN: SMCAR-AEE	1
SMCAR-AES, BLDG. 321	1
SMCAR-AET-O, BLDG. 351N	1
SMCAR-CC	1
SMCAR-CCP-A	1
SMCAR-FSA	1
SMCAR-FSM-E	1
SMCAR-FSS-D, BLDG. 94	1
SMCAR-IMI-I (STINFO) BLDG. 59 PICATINNY ARSENAL, NJ 07806-5000	2
DIRECTOR US ARMY BALLISTIC RESEARCH LABORATORY ATTN: SLCBR-DD-T, BLDG. 305 ABERDEEN PROVING GROUND, MD 21005-5066	1
DIRECTOR US ARMY MATERIEL SYSTEMS ANALYSIS ACTV ATTN: AMXSY-MP ABERDEEN PROVING GROUND, MD 21005-5071	1
COMMANDER HQ, AMCCOM ATTN: AMSMC-IMP-L ROCK ISLAND, IL 61299-6000	1
COMMANDER ROCK ISLAND ARSENAL ATTN: SMCRI-ENM ROCK ISLAND, IL 61299-5000	1
MIAC/CINDAS PURDUE UNIVERSITY P.O. BOX 2634 WEST LAFAYETTE, IN 47906	1
COMMANDER US ARMY TANK-AUTMV R&D COMMAND ATTN: AMSTA-DDL (TECH LIB) WARREN, MI 48397-5000	1
COMMANDER US MILITARY ACADEMY ATTN: DEPARTMENT OF MECHANICS WEST POINT, NY 10996-1792	1
US ARMY MISSILE COMMAND REDSTONE SCIENTIFIC INFO CTR ATTN: DOCUMENTS SECT, BLDG. 4484 REDSTONE ARSENAL, AL 35898-5241	2
COMMANDER US ARMY FGN SCIENCE AND TECH CTR ATTN: DRXST-SD 220 7TH STREET, N.E. CHARLOTTESVILLE, VA 22901	1
COMMANDER US ARMY LABCOM MATERIALS TECHNOLOGY LAB ATTN: SLCMT-IML (TECH LIB) WATERTOWN, MA 02172-0001	2

NOTE: PLEASE NOTIFY COMMANDER, ARMAMENT RESEARCH, DEVELOPMENT, AND ENGINEERING CENTER, US ARMY AMCCOM, ATTN: BENET LABORATORIES, SMCAR-CCB-TL, WATERVLIET, NY 12189-4050, OF ANY ADDRESS CHANGES.

TECHNICAL REPORT EXTERNAL DISTRIBUTION LIST (CONT'D)

	NO. OF COPIES
COMMANDER US ARMY LABCOM, ISA ATTN: SLCIS-IM-TL 2800 POWDER MILL ROAD ADELPHI, MD 20783-1145	1
COMMANDER US ARMY RESEARCH OFFICE ATTN: CHIEF, IPO P.O. BOX 12211 RESEARCH TRIANGLE PARK, NC 27709-2211	1
DIRECTOR US NAVAL RESEARCH LAB ATTN: MATERIALS SCI & TECH DIVISION CODE 26-27 (DOC LIB) WASHINGTON, D.C. 20375	1 1
COMMANDER AIR FORCE ARMAMENT LABORATORY ATTN: AFATL/MN EGLIN AFB, FL 32542-5434	1
COMMANDER AIR FORCE ARMAMENT LABORATORY ATTN: AFATL/MNF EGLIN AFB, FL 32542-5434	1
DIRECTOR US ARMY BALLISTIC RESEARCH LABORATORY ATTN: SLCBR-IB-M (DR. BRUCE BURNS) ABERDEEN PROVING GROUND, MD 21005-5066	1

NOTE: PLEASE NOTIFY COMMANDER, ARMAMENT RESEARCH, DEVELOPMENT, AND ENGINEERING CENTER, US ARMY AMCCOM, ATTN: BENET LABORATORIES, SMCAR-CCB-TL, WATERVLIET, NY 12189-4050, OF ANY ADDRESS CHANGES.